# Anharmonicity and Quantum Effects in Thermal Expansion of an Invar Alloy

Toshihiko Yokoyama[1,2,*] and Keitaro Eguchi[2]

[1]*Department of Materials Molecular Structure, Institute for Molecular Science, Myodaiji-cho, Okazaki, 444-8585, Japan*
[2]*Department of Structural Molecular Science, The Graduate University for Advanced Studies (Sokendai), Myodaiji-cho, Okazaki, 444-8585, Japan*

(Received 21 May 2011; published 3 August 2011)

We have investigated the anharmonicity and quantum effects in the Invar alloy $Fe_{64.6}Ni_{35.4}$ that shows anomalously small thermal expansion. We have performed Fe and Ni *K*-edge extended x-ray-absorption fine-structure spectroscopic measurements and the computational simulations based on the path-integral effective-classical-potential theory. The first nearest-neighbor (NN) shells around Fe show almost no thermal expansion, while those around Ni exhibit meaningful but smaller expansion than that of fcc Ni. At low temperature, the quantum effect is found to play an essentially important role, which is confirmed by comparing the quantum-mechanical simulations to the classical ones. The anharmonicity (asymmetric distribution) clearly exists for all the first NN shells as in normal thermal expansion systems, implying the breakdown of the direct correspondence between thermal expansion and anharmonicity.

DOI: 10.1103/PhysRevLett.107.065901 PACS numbers: 65.40.De, 61.05.cj, 63.20.Ry, 64.60.De

Anomalously small thermal expansion over a wide temperature range in an iron-nickel alloy with a nickel concentration of around 35% was discovered by Guillaume in 1897 [1]. The effect is well known as the Invar effect and has been utilized in various kinds of industrial products. Other physical properties such as elastic constants and magnetization show also anomalous behaviors [2–4]. It has been recognized that the effect originates from magnetism. However, there are still many scientific papers published concerning the origins of the Invar effect, thus implying a lack of a full understanding of the effect. A basic concept of the Invar effect is that there exist at least two types of electronic states in Fe, typically high-spin (HS) and low-spin (LS) states [2,5]. In this two-state model, the equilibrium potential energy is lower in the HS state than in the LS one, while the equilibrium atomic radius is larger in the former. This results in the compensation of thermal expansion due to increasing density of the LS state at higher temperature. A recent *ab initio* electronic structure calculation at 0 K, however, reveals very complicated electronic configurations in a smaller volume region [6]. Computational simulations at finite temperatures have also been carried out for the understanding of magnetization and thermal expansion [7–11]. There have been, however, no reports concerning quantum-mechanical dynamics calculations, such as path-integral Monte Carlo (MC) simulations, to the best of our knowledge, although in general thermal expansion inherently results from anharmonic vibration, to which the quantum effect is essentially important at low temperature.

In this Letter, we will present the experimental results of the local thermal expansion and the anharmonic behavior around Fe and Ni by measuring Fe and Ni *K*-edge extended x-ray-absorption fine-structure (EXAFS) spectra of the Invar alloy. EXAFS is a very powerful tool for the characterization of local thermodynamic properties and has extensively been applied to various kinds of thermodynamic systems [12–24]. In the present work, it is found that the first nearest-neighbor (NN) bond distance around Fe shows almost no thermal expansion in the temperature range of 12.5–300 K, while the one around Ni also gives significantly smaller expansion than that for the fcc Ni. It is well established that the vibrational anharmonicity leads to thermal expansion in normal materials. The present system is, however, found to give a pretty normal anharmonicity that was evaluated from the asymmetry of the pair distribution function. We will also present the MC simulation results of thermal expansion and vibrational anharmonicity obtained by the path-integral effective-classical-potential (PIECP) theory [21–23,25] within the simple two-state (HS + LS) model. It is revealed by comparing the results given by the classical theory that the quantum effect drastically contributes to the Invar effect at low temperature ($< 100$ K). Moreover, all the bonds of Ni-Ni, Ni-Fe, and Fe-Fe pairs exhibit significant suppression of thermal expansion, although the Ni potential itself is not affected by the change of the Fe HS-LS state.

The Fe and Ni *K*-edge EXAFS spectra of a pinholeless $Fe_{64.6}Ni_{35.4}$ foil 8 $\mu$m thick were recorded at Beamline 9C of Photon Factory in High Energy Accelerator Organization (KEK-PF) [26] with the transmission mode using a Si(111) double crystal monochromator. Ionization chambers filled with 100% $N_2$ and 50% Ar in $N_2$ were used to measure the incident and transmitted x-ray intensities, respectively. The measurement temperature range was 12.5–300 K. For comparison, Cu and Ni *K*-edge EXAFS spectra of fcc Cu and Ni metal foils were taken. The temperature was measured by a calibrated Si diode placed near the sample and also verified by the temperature dependence of the Cu *K*-edge EXAFS of fcc Cu.

 

The EXAFS oscillation functions $k^3\chi(k)$ ($k$ the photoelectron wave number) were obtained by the standard procedures as the background subtraction and the normalization with atomic absorption coefficients. The $k^3\chi(k)$ functions were subsequently Fourier transformed, Fourier filtered for the peaks of interest (the first NN shell in the present study), and were finally curve-fitted in $k$ space. Note here that the neighboring atoms of surrounding Fe or Ni were not distinguished because of only a small difference of the backscattering amplitudes between Fe and Ni, and therefore the resultant values obtained experimentally are the average ones for each x-ray absorbing atom. The bond distance $R$, the mean square relative displacements $C_2 = \langle (r - R)^2 \rangle$, and the mean cubic relative displacements $C_3 = \langle (r - R)^3 \rangle$ were obtained. $C_2$ and $C_3$ correspond to the thermal and static variance of the bond distance and the asymmetry of the pair distribution function, respectively [27]. To evaluate the relative quantities like thermal expansion, empirical analysis using the lowest temperature data as a reference was conducted, while the determination of the absolute values was carried out by employing the FEFF8 [28] standards that were obtained by the calculations of clusters assuming some randomly distributed alloy structures.

PIECP MC simulations within the low coupling approximation [22,25] were performed under a constant number of particles, pressure, and temperature ($NPT$) condition. The constant-pressure condition is essentially important to reveal thermal expansion [14,24]. Although the PIECP theory can treat only periodic lattices [22,25] and is strictly not applicable to the present alloy system with random distribution, the Invar alloy exhibits clear fcc structure and the atomic weights of Fe and Ni are not very different, allowing us to adopt the theory to the present simulation. The total number of atoms was 500 ($5^3$ fcc cubic unit cells), and the distributions of Fe and Ni were chosen randomly. Eleven types of the superlattices were simulated and the results were averaged to provide consequent physical quantities. The potentials of Fe and Ni were based on the empirical embedded-atom method (EAM) [29,30]. The potential parameters of Ni were optimized by using known thermodynamic quantities like elastic constants [30]. Those of Fe were assumed by referring to the literature [31–33] and also the present experimental results. For comparison, the MC simulations based on the classical thermodynamics and also the PIECP simulations using only the HS potential were carried out. More detailed descriptions of the data analysis computational procedures are found in the Supplemental Material [34].

Figure 1 shows the thermal expansion of the 1st NN bond distances determined by the present EXAFS. The dashed line corresponds to the experimental equilibrium distance $R_{\text{lattice}} = a_0/\sqrt{2}$ ($a_0$ is the lattice constant determined by the x-ray diffraction [35]). The solid line is the bond distance $R_{\text{bond}}$ estimated within the harmonic approximation as $R_{\text{bond}} = R_{\text{lattice}} + \langle u_\perp^2 \rangle / R_{\text{lattice}}$, where $\langle u_\perp^2 \rangle$ is the average squared displacement of each atom along the perpendicular direction to the corresponding bond axis. The difference of the distance between $R_{\text{lattice}}$ and $R_{\text{bond}}$ originates from the vibration perpendicular to the equilibrium bond direction [17–20]. $R_{\text{bond}}$ is always slightly larger than $R_{\text{lattice}}$. The $\langle u_\perp^2 \rangle$ can be evaluated using the correlated Debye model [36] with the Debye temperature of $\Theta_D = 430$ K, which was estimated from the present temperature dependence of $C_2$. The fcc Cu and Ni metals show normal thermal expansion in good agreement with estimated $R_{\text{bond}}$, indicating high accuracy of the present analysis as in the previous reports [18–20,22–24].

In the Invar alloy, thermal expansion is hardly seen in the local structure around Fe, while that around Ni is observed clearly. The magnitude of thermal expansion around Ni is, however, significantly smaller than that of fcc Ni, indicating the suppression of thermal expansion around Ni as well as Fe. As we expected from the two-state model given by Weiss [2], almost no thermal expansion around Fe can be ascribed to the direct effect of the increasing population of the LS state in Fe with increasing temperature. On the other hand, the behavior around Ni may be attributed to the indirect effect in the two-state model. Although Ni is likely to expand normally with the temperature rise, this is also suppressed by the almost fixed lattice constant. This will be further discussed in detail below.

Figure 2 shows the simulated bond distances and the lattice constants by the PIECP and classical MC methods. Figure 2(a) gives the binding energies of Invar $Fe_{65}Ni_{35}$ and fcc Fe at a temperature of 0 K as a function of the 1st NN distance. In the present atomic potentials, the fcc Fe system shows that the LS state is more stable by 8.0 meV

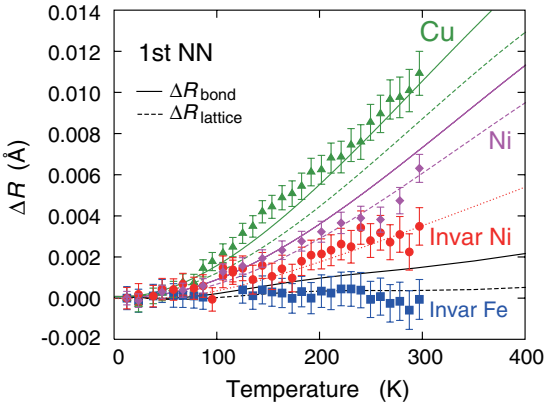


FIG. 1 (color online). Experimentally observed thermal expansion of the 1st NN bond distances for the Invar alloy (red circle for Ni and blue square for Fe), fcc Ni (purple diamond), and fcc Cu (green triangle). The dashed lines are the 1st NN distance estimated from the lattice constant, while the solid lines are the corresponding bond distances corrected within the harmonic vibration (see the text for details ). The red dotted line is a guide to the eye for the bond distance around Ni in the Invar alloy.

than the HS state with the bond distances of $R^{HS} = 2.530$ Å and $R^{LS} = 2.492$ Å, while the Invar case exhibits a more stable HS state by 25.0 meV with the bond distances of $R^{HS} = 2.530$ Å and $R^{LS} = 2.490$ Å. In Figs. 2(b)–2(d), the agreement between the PIECP and experiments is good: almost no thermal expansion around Fe and meaningful thermal expansion around Ni. On the contrary, the classical method is found to give fatal discrepancies at low temperature below ~100 K; the bond and lattice distances significantly increase with the temperature rise. These findings imply the essential importance of the quantum effect, which is recognized as a zero-point vibration.

To get further insights into local thermal expansion, the bond distance of each component (Fe-Fe, Ni-Ni and Ni-Fe) pair is shown in Fig. 3. In this plot, the PIECP MC results, by using only the HS Fe state, are also depicted to recognize hypothetical normal thermal expansion in this system. As expected, the Fe-Fe pair shows the largest discrepancies between the two-state (HS + LS) and the HS-only models. This is caused by the increasing population of the Fe LS state with the temperature rise, yielding compensation of the thermal expansion with the one originating from anharmonic vibration. The most important finding in Fig. 3 is that even Ni-Ni and Ni-Fe pairs exhibit significant suppression of thermal expansion. This is consistent with the above experimental finding that thermal expansion around Ni is noticeably suppressed compared to that of fcc Ni. Although Ni does not change its electronic configuration depending on temperature and may tend to expand because of anharmonic vibration, the Ni-Ni or Ni-Fe bond expansion is significantly suppressed due to the anomalously small expansion of the lattice. Interestingly, the suppression of the thermal expansion seems more significant in the Ni-Fe bond than in the Ni-Ni bond. This can be explained by the fact that the Fe atom surrounded by many Ni atoms tends to maintain the HS state. In the present EAM potentials, the energy difference between the HS and LS states is determined by the sum of the $d$ electron density of surrounding atoms at the Fe site. The $d$ electron density at the 1st NN distance is smaller in Ni than in Fe because of larger nuclear charge in Ni, leading to more probability of the HS state in Fe surrounded by more Ni atoms. Furthermore, the Ni-Ni bond is noticeably softer than the Ni-Fe bond and is more likely to match the lattice parameter. These effects consequently yield smaller thermal expansion in the Ni-Ni bond than the Ni-Fe one.

Finally, let us discuss the third-order anharmonicity in the Invar alloy. Figure 4 shows the mean cubic relative displacements $C_3$ for the average 1st NN shells around Fe and Ni,

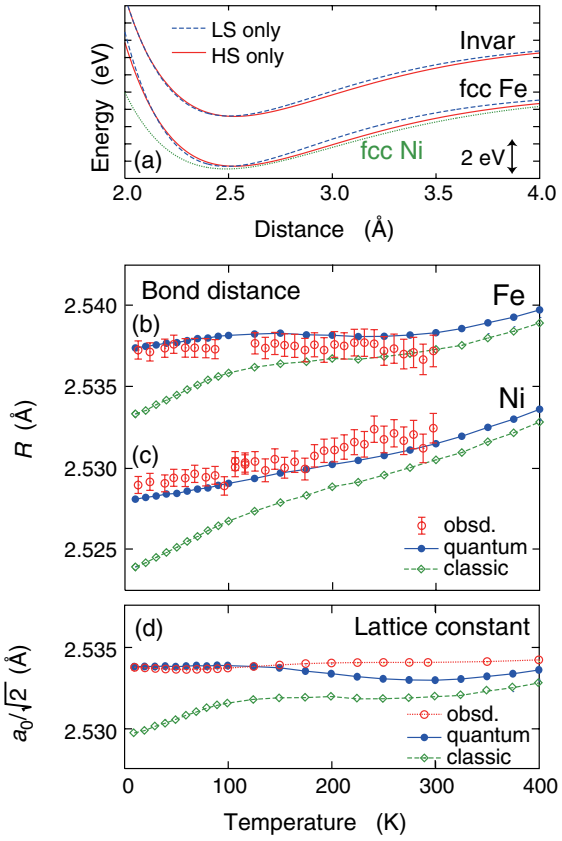


FIG. 2 (color online). (a) Binding energies of Invar $Fe_{64.6}Ni_{35.4}$ (top lines), fcc Fe (bottom lines), and fcc Ni (bottom, green dotted line) as a function of the 1st NN distance at a temperature of 0 K. For Fe, two types of the potentials for the HS (red solid line) and LS (blue dashed line) states are depicted. (b),(c) Simulated 1st NN bond distance around Fe (b) and Ni (c) given by the PIECP (blue circles and solid line, quantum) and the classical MC (green diamond and dashed line, classic) methods, together with the experimental EXAFS data (red open circle with an error bar). (d) Equilibrium 1st NN distance ($a_0/\sqrt{2}$) given by the PIECP and classical MC simulations, together with the experimental literature data (red circle and dotted line) [35].

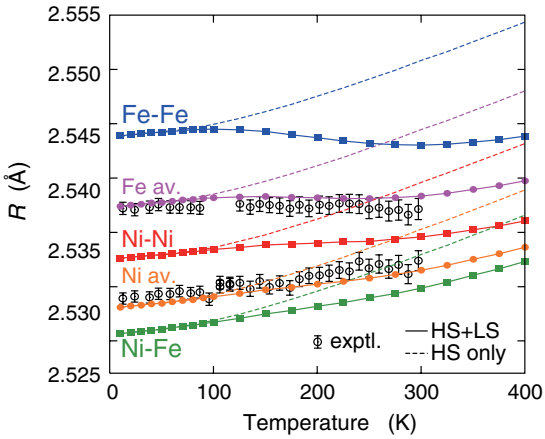


FIG. 3 (color online). Simulated bond distances of Fe-Fe (blue square and solid line), Ni-Ni (red square and solid line), and Ni-Fe (green square and solid line) pairs, together with the average ones around Fe (pink circle and solid line) and Ni (orange circle and solid line). The experimental data for the average one around Fe and Ni are again shown. The dashed lines are the PIECP results by using only the HS state in Fe.

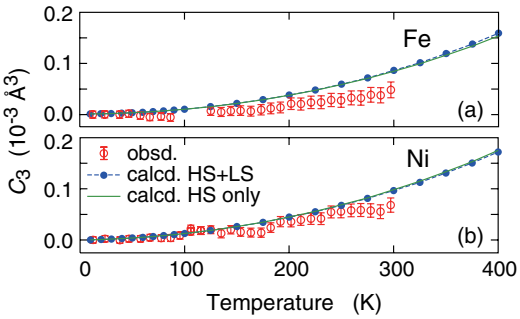


FIG. 4 (color online). Mean cubic relative displacement $C_3$ given by the experimental EXAFS (red open circle with an error bar) and by the PIECP simulations using the two-state (blue circle and dashed line) and the HS-only (green solid line) models for the average 1st NN bonds around Fe (a) and Ni (b).

respectively. The agreement between the experiments and the PIECP simulations is not perfect, but $C_3$ increases gradually with the increase in temperature for both the Fe and Ni data. Clear anharmonicity in the Invar alloy is thus confirmed by comparing the PIECP simulations between the two-state (HS + LS) and HS-only models. Both the simulated data exhibit essentially the same $C_3$ values, implying no suppression of $C_3$ due to the contribution of the LS state, as observed in the thermal expansion. Since the asymmetric radial distribution for the 1st NN shell almost exclusively originates from the anharmonic interatomic potential [37–39], the present result implies that the third-order anharmonicity clearly exists even in the case of no thermal expansion. Note that in the present PIECP simulations within the low coupling approximation, the quantum effect in $C_3$ is not properly taken into consideration because of the neglect of the phonon-phonon coupling. The important qualitative finding of the presence of $C_3$ without thermal expansion is, however, clearly exemplified.

We are grateful for the partial financial support of Grant-in-Aid for Scientific Research (A) (No. 22241029) from Japan Society for the Promotion of Science (JSPS). The EXAFS measurements at Photon Factory have been performed under the approval of Photon Factory Program Advisory Committee (PF-PAC No. 2010G551).

*yokoyama@ims.ac.jp

[1] C. E. Guillaume, C.R. Hebd. Seances Acad. Sci. **125**, 235 (1897).
[2] R. J. Weiss, Proc. Phys. Soc. London **82**, 281 (1963).
[3] M. Shiga, J. Phys. Soc. Jpn. **22**, 539 (1967).
[4] S. Chikazumi, J. Magn. Magn. Mater. **10**, 113 (1979).
[5] M. Matsui and S. Chikazumi, J. Phys. Soc. Jpn. **45**, 458 (1978).
[6] M. van Schilfgaarde, I. A. Abrikosov, and B. Johansson, Nature (London) **400**, 46 (1999).
[7] D. G. Rancourt and M.-Z. Dang, Phys. Rev. B **54**, 12 225 (1996).
[8] J. M. Wesselinowa, I. P. Ivanov, and P. Entel, Phys. Rev. B **55**, 14 311 (1997).
[9] R. Meyer and P. Entel, Phys. Rev. B **57**, 5140 (1998).
[10] M. E. Grunera, R. Meyer, and P. Entel, Eur. Phys. J. B **2**, 107 (1998).
[11] K. Lagarec and D. G. Rancourt, Phys. Rev. B **62**, 978 (2000).
[12] A. Di Cicco, A. Trapananti, S. Faggioni, and A. Filipponi, Phys. Rev. Lett. **91**, 135505 (2003).
[13] A. Filipponi, A. Di Cicco, and S. De Panfilis, Phys. Rev. Lett. **83**, 560 (1999).
[14] A. Di Cicco, A. Filipponi, J. P. Itié, and A. Polian, Phys. Rev. B **54**, 9086 (1996).
[15] L. Wenzel, D. Arvanitis, H. Rabus, T. Lederer, K. Baberschke, and G. Comelli, Phys. Rev. Lett. **64**, 1765 (1990).
[16] H. Wende, D. Arvanitis, M. Tischer, R. Chauvistre, H. Henneken, F. May, and K. Baberschke, Phys. Rev. B **54**, 5920 (1996).
[17] J. M. Tranquada and R. Ingalls, Phys. Rev. B **28**, 3520 (1983).
[18] G. Dalba, P. Fornasini, R. Grisenti, and J. Purans, Phys. Rev. Lett. **82**, 4240 (1999).
[19] S. a Beccara, G. Dalba, P. Fornasini, R. Grisenti, A. Sanson, and F. Rocca, Phys. Rev. Lett. **89**, 025503 (2002).
[20] P. Fornasini, S. a Beccara, G. Dalba, R. Grisenti, A. Sanson, M. Vaccari, and F. Rocca, Phys. Rev. B **70**, 174301 (2004).
[21] T. Fujikawa, T. Miyanaga, and T. Suzuki, J. Phys. Soc. Jpn. **66**, 2897 (1997).
[22] T. Yokoyama, Phys. Rev. B **57**, 3423 (1998).
[23] T. Yokoyama, J. Synchrotron Radiat. **8**, 87 (2001).
[24] T. Yokoyama, T. Ohta, and H. Sato, Phys. Rev. B **55**, 11320 (1997).
[25] A. Cuccoli, R. Giachetti, V. Tognetti, R. Vaia, and P. Verrucchi, J. Phys. Condens. Matter **7**, 7891 (1995) and references therein.
[26] M. Nomura, http://pfwww.kek.jp/users_info/station_spec/xafsbl/9c/bl9c_e.html.
[27] G. Bunker, Nucl. Instrum. Methods Phys. Res. **207**, 437 (1983).
[28] A. L. Ankudinov, B. Ravel, J. J. Rehr, and S. D. Conradson, Phys. Rev. B **58**, 7565 (1998).
[29] M. S. Daw and M. I. Baskes, Phys. Rev. B **29**, 6443 (1984).
[30] S. M. Foiles, Phys. Rev. B **32**, 3409 (1985).
[31] Y. Mishin, M. J. Mehl, and D. A. Papaconstantopoulos, Acta Mater. **53**, 4029 (2005).
[32] S. L. Dudarev and P. M. Derlet, J. Phys. Condens. Matter **17**, 7097 (2005); **19**, 239001(E) (2007).
[33] M. Müller, P. Erhart, and K. Albe, J. Phys. Condens. Matter **19**, 326220 (2007).
[34] See Supplemental Material at http://link.aps.org/supplemental/10.1103/PhysRevLett.107.065901 for more detailed data analysis and computational procedures.
[35] *Thermodynamical Properties of Matter*, edited by Y. S. Touloukian, R. K. Kirby, R. E. Taylor, and T. Y. R. Lee (Plenum, New York, 1975), Vol. 12, p. 848.
[36] G. Beni and P. M. Platzman, Phys. Rev. B **14**, 1514 (1976).
[37] H. Rabus, Ph.D. thesis, Freie Universität Berlin, 1991.
[38] A. I. Frenkel and J. J. Rehr, Phys. Rev. B **48**, 585 (1993).
[39] T. Yokoyama, J. Synchrotron Radiat. **6**, 323 (1999).